THE JOURNAL OF BIOLOGICAL CHEMISTRY VOL. 291, NO. 2, pp. 681–690, January 8, 2016

The A-kinase Anchoring Protein GSKIP Regulates GSK3β Activity and Controls Palatal Shelf Fusion in Mice*

Received for publication, October 29, 2015, and in revised form, November 16, 2015 Published, JBC Papers in Press, November 18, 2015, DOI 10.1074/jbc.M115.701177

Veronika Anita Deák[‡], Philipp Skroblin[‡], Carsten Dittmayer[§], Klaus-Peter Knobeloch[¶], Sebastian Bachmann[§], and Enno Klussmann[‡‖1]

From the [‡]Max Delbrück Center for Molecular Medicine in the Helmholtz Association (MDC), Robert-Rössle-Strasse 10, 13125 Berlin, the [§]Institute of Anatomy, Charité University Medicine, Philippstrasse 12, 10115 Berlin, Germany, the [¶]Institute for Neuropathology, University of Freiburg, Breisacher Strasse 64, 79106 Freiburg, and the [‖]DZHK (German Centre for Cardiovascular Research), partner site Berlin, Oudenarder Strasse 16, 13347 Berlin, Germany

A-kinase anchoring proteins (AKAPs) represent a family of structurally diverse proteins, all of which bind PKA. A member of this family is glycogen synthase kinase 3β (GSK3β) interaction protein (GSKIP). GSKIP interacts with PKA and also directly interacts with GSK3β. The physiological function of the GSKIP protein *in vivo* is unknown. We developed and characterized a conditional knock-out mouse model and found that GSKIP deficiency caused lethality at birth. Embryos obtained through Caesarean section at embryonic day 18.5 were cyanotic, suffered from respiratory distress, and failed to initiate breathing properly. Additionally, all GSKIP-deficient embryos showed an incomplete closure of the palatal shelves accompanied by a delay in ossification along the fusion area of secondary palatal bones. On the molecular level, GSKIP deficiency resulted in decreased phosphorylation of GSK3β at Ser-9 starting early in development (embryonic day 10.5), leading to enhanced GSK3β activity. At embryonic day 18.5, GSK3β activity decreased to levels close to that of wild type. Our findings reveal a novel, crucial role for GSKIP in the coordination of GSK3β signaling in palatal shelf fusion.

PKA is a serine/threonine kinase that controls a wide variety of cellular processes (1, 2). A-kinase anchoring proteins (AKAPs)[2] directly interact with the regulatory (R) subunits of PKA and facilitate PKA phosphorylation of its substrates at specific intracellular compartments (3–5). This coordinating function of AKAPs is not limited to PKA signaling; AKAPs directly bind further signaling proteins and thereby coordinate crosstalk between multiple signaling pathways. An example is the AKAP glycogen synthase kinase 3β (GSK3β) interaction protein (GSKIP). GSKIP directly interacts with PKA and GSK3β (6), but its functions have not been determined. Recently, an autosomal dominant 700-kb duplication encompassing the Gskip gene was identified in humans; this alteration causes a predisposition for myeloid malignancies, indicating a likely role in tumorigenesis (7).

To date, functional analyses of the GSKIP protein have been limited to *in vitro* and overexpression studies. GSKIP contains a structurally conserved PKA-binding domain (amino acids 28–52) that is characteristic for AKAPs and specifically binds regulatory RII subunits of PKA. GSK3β binds GSKIP at its C-terminal conserved GSK3β-binding domain (GID; amino acids 115–139) (6, 8). The interaction between GSKIP and GSK3β through the GID is conserved among vertebrates and invertebrates, whereas its interaction with PKA RII subunits is restricted to vertebrates. This indicates that it functions as an AKAP exclusively in vertebrates (6).

GSK3 is a highly conserved serine-threonine kinase involved in a plethora of cellular processes including glycogen metabolism, proliferation, differentiation, and development. It is found in the cytosol, nucleus, and mitochondria of all eukaryotic cells (9). There are two homologous genes encoding two isoforms of GSK3, GSK3α (51 kDa) and GSK3β (47 kDa). Both isoforms of GSK3 are constitutively active and phosphorylate primed substrates, *i.e.* substrates that have been pre-phosphorylated by casein kinase 1 (CK1), MAPK, ERK, or other kinases (reviewed in Ref. 10). Despite their structural similarities, GSK3α and GSK3β are functionally non-redundant (11). GSK3β activity is inhibited by Ser-9 phosphorylation (12). We have shown that GSKIP facilitates the inhibitory phosphorylation of GSK3β at Ser-9 by PKA when overexpressed in cultured cells (6).

GSK3β is a component of the canonical Wnt signaling pathway, which plays a critical role in embryonic development. Canonical Wnt signaling controls essential processes such as body axis patterning, cell proliferation, epithelial cell fate, and cell migration (13, 14). Studies of Wnt-related knock-out mouse models revealed that the dysregulation of *Lrp6* (15), *Gpr177 (16)*, *Wnt5a* (17), and *Wnt9b* (18) induces palatal clefting, an abnormal development of facial structure (19). Wnt signaling is activated by binding of Wnt ligands to receptor complexes at the plasma membrane that consist of LRP5/6 transmembrane proteins and G protein-like receptors of the Frizzled (Fz) family. The knock-out of *Lrp6* resulted in defects in orofacial development and disruptions of other embryonic features. $Lrp6^{-/-}$ animals exhibit hypoplasia of the upper lip and midline cleft of the mandible at embryonic day 13.5 (E13.5), and the absence of the primary palate at E16.5 (15), giving rise to a cleft lip and palate phenotype. Gpr177 (mouse ortholog of

* This work was supported by grants from the Else Kröner-Fresenius-Stiftung (2013_A145) (to E. K.), and the German-Israeli Foundation (G.I.F. I-1210-286.13/2012) (to E. K.). The authors declare that they have no conflicts of interest with the contents of this article.

[1] To whom correspondence should be addressed. Tel.: 49-30-9406-2596; Fax: 49-30-9406-2593; E-mail: enno.klussmann@mdc-berlin.de.

[2] The abbreviations used are: AKAP, A-kinase anchoring protein; GSK3α/β, glycogen synthase kinase 3α/β; GSKIP, GSK3β interaction protein; C, catalytic subunit of PKA; R, regulatory subunit of PKA; GID, GSK3β-binding domain; E, embryonic day; P, postnatal day.

Wntless) is a ubiquitous transmembrane protein directly activated by β-catenin and TCF/LEF-dependent transcription. Gpr177-Wnt complexes enhance Wnt production in a positive feedback loop. Mice deficient for mesenchymal Gpr177 in craniofacial neural crest cells display a secondary cleft palate, which is mainly due to aberrant cell proliferation and increased cell death in the palatal shelves (16). *Wnt5a* deficiency also causes a secondary cleft palate. These mice exhibited altered cell proliferation patterns and a lack of directional cell migration along the anterior-posterior axis within the developmental palate (17). 50% of *Wnt9b* knock-out mice display a cleft lip and palate (20), and inactivating mutations in *Wnt9* lead to a lethal syndrome of fully penetrant vestigial kidneys and the lack of reproductive ducts (21).

In canonical Wnt signaling, GSK3β assembles with Axin, β-catenin, adenomatous polyposis coli (APC), and CK1 in the destruction complex located in the cytosol. In the absence of a Wnt signal, GSK3β phosphorylates β-catenin (22–26), thus promoting its ubiquitination and proteasomal degradation. Activation of Wnt signaling leads to the inhibition of GSK3β through phosphorylation, allowing β-catenin to accumulate and induce transcription of Wnt target genes. Inhibitors of GSK3β include GSKIP and GSKIPtide, a peptide encompassing the GID and corresponding to amino acid residues 115–139 of GSKIP; they activate the canonical Wnt signaling pathway in neuroblastoma SH-SY5Y cells (27). The overexpression of GSKIP induces β-catenin accumulation in the cytoplasm and in the nucleus and down-regulates N-cadherin expression, thus blocking neurite outgrowth during retinoic acid-mediated differentiation of the cells (8).

Despite considerable knowledge of GSKIP functions gained in cell culture systems, its physiological relevance remains unknown. Here we generated and characterized a new conditional *Gskip* knock-out mouse to gain insights into its function. GSKIP deficiency is associated with the modulation of GSK3β activity during development and a cleft palate.

Experimental Procedures

Mice—To generate conditional *Gskip* mice ($Gskip^{fl/fl}$), exon 2 was flanked with loxP sites via homologous recombination in embryonic stem cells. Therefore, the targeting vector pPNT-FRT3-gskip was transfected into E14.1 mouse embryonic stem cells, and clones harboring the expected mutation (clone H3) were identified by Southern analysis. Germline chimeras were generated by injection in blastocyst using standard procedures. Heterozygous $Gskip^{+/-}$ mice lacking exon 2 were obtained upon mating to the general B6.C-Tg(CMV-cre)1Cgn/J Cre deleter strain (28). Cre-mediated deletion results in the deletion of a genomic region encoding 86 out of a total of 119 amino acids of GSKIP including the start codon, thus causing a *Gskip* null mutation ($Gskip^{-/-}$). $Gskip^{+/-}$ as well as $Gskip^{flx/wt}$ mice were backcrossed to C57BL/6 animals for at least 10 generations. For genotyping, the following primers were used: GSKIP-fw (see Fig. 1*C*, *red*), 5′AAA AGT TTA AAA AGG TCT GGA AAG C 3′ in combination with either GSKIP-rev (see Fig. 1*C*, *blue*), 5′ TAG TGT TGC TTT TAA GAC AGG GTT T 3′, or loxP-rev (see Fig. 1*C*, *green*), 5′ TCT GCA AGA AAG GAG TAA CAG ATT T 3′.

Animal Husbandry—All mice were housed and maintained in a specific pathogen-free environment in the animal facility of the Max Delbrück Center for Molecular Medicine according to the recommendations of the Federation of European Laboratory Animal Science Associations (FELASA), with chow and water *ad libitum* in air-conditioned rooms at 22–23 °C with a standard 12-h light/dark cycle. Mice were weaned 4 weeks after birth and ear-punched for numbering, and female and male mice were separated. After genotyping, one or two females were placed in a cage with one male for standard breeding. All procedures were carried out in accordance with the ethical guidelines of the Landesamt für Gesundheit und Soziales (LaGeSo), Berlin, Germany. Embryo analysis was conducted as approved by License G 0361/13.

Embryo Analysis—Timed matings were set up by intercrossing $Gskip^{+/-}$ animals for the generation of homozygous $Gskip^{-/-}$ embryos. Genotype ratios were calculated and compared with expected Mendelian ratios to determine the time point of death of $Gskip^{-/-}$ mice. E18.5 animals were born through Caesarean sectioning, and P0 animals were abdominally delivered. E18.5 and P0 embryos were weighed, lungs were carefully dissected, and their ability to float on PBS was tested as readout for air in the lung. Dissections for optical inspections and staining procedures were carried out for determination of gross morphological abnormalities.

Tissue Lysis and Western Blot Analysis—Organs and whole embryos were ground to powder in liquid N_2 and resuspended in standard radioimmunoprecipitation assay buffer containing protease and phosphatase inhibitors (Roche Diagnostics, Mannheim, Germany). Homogenates were sonicated and centrifuged, and total protein concentrations of supernatants were determined using the Coomassie Plus Bradford protein assay (Thermo Scientific). Proteins (10–25 μg) were separated by 12% SDS-PAGE and blotted onto PVDF membranes. Membranes were blocked 1 h at room temperature with 1% BSA in TBS-T and then incubated overnight at 4 °C with primary antibodies directed against: GSKIP (custom-made, used as described previously (6)), cyclin D1 (Abcam), GSK3, pGSK3-Ser(P)-9, β-catenin, Axin1, and GAPDH (Cell Signaling Technology), and PKA-RIIα and PKA-C (BD Biosciences). The blots were washed and incubated with HRP-conjugated secondary antibodies (Jackson ImmunoResearch Laboratories/Dianova) and Western chemiluminescence HRP substrate (Merck Millipore). Signals were visualized using an Odyssey imaging system (LI-COR Biosciences). Signals were semi-quantitatively analyzed using the ImageJ 1.47v software (National Institutes of Health). For the evaluation of GSK3β protein activity, the ratio was calculated between the signal intensity measured for inactive GSK3β phosphorylated at Ser-9 (inactive) to the signal for total GSK3β (both active and inactive forms). The ratios were normalized to wild type controls and determined as -fold changes as compared with wild type.

Isolation of Total RNA and Real-time Reverse Transcription-PCR—Total RNA was isolated from homogenized mouse tissue using TRIzol (Sigma-Aldrich) and chloroform according to the manufacturer's protocol. RNA (100–1,000 ng) was reverse-transcribed according to the SuperScript III first-strand synthesis kit protocol (Invitrogen, Thermo Fisher Scien-

tific). Duplex-real-time RT-PCR was performed using the TaqMan system and a Bio-Rad iCycler and the comparative ΔΔCT method for relative gene expression analysis comparing wild type and *Gskip*$^{-/-}$ mouse tissue. GAPDH was included as a control.

Hematoxylin-Eosin, Azan, and Whole-mount Alizarin Red/Alcian Blue Stain—For histologic analysis, freshly dissected embryos and isolated heads were rinsed briefly in PBS, fixed in 4% paraformaldehyde, and embedded in paraffin. H&E and Azan stain were used on sections of paraffin-embedded whole embryos or skulls for morphological inspection according to standard protocols. In accordance with ethical guidelines, animals were sacrificed by decapitation; hence whole-body sections lack the skull. For microscopic evaluation, a digital Keyence BZ-8100E bright-field microscope was used. For whole-mount staining of skulls, E18.5 embryos were dissected and decapitated. The lower jaw of the skull including the tongue was carefully removed, and the remaining upper part of the skull eviscerated and fixed in 99% ethanol at room temperature for 2–5 days (in a total volume of 15 ml per skull). The material was processed by a 24-h incubation in acetone at room temperature for fat removal. Samples were rinsed once in distilled water. Each skull was transferred to a new tube containing Alizarin red/Alcian blue double staining solution (0.3% Alcian blue, 0.1% Alizarin red) optimized according to Erdoğan *et al.* (29). Staining was performed at 40 °C for 4 days under rotation. Skulls were briefly washed and transferred into 1.5% aqueous KOH solution for 4 days for clearing. The skulls were transferred into an aqueous solution of 20% glycerol containing 1% KOH until the skulls were clearly visible through the surrounding tissue. Cleared specimens were placed successively into 50, 80, and 100% glycerol for 3–5 days each for long-term storage and imaging. Stained skulls were viewed under a stereomicroscope connected to a Leica DFC 495 camera.

Statistical Analysis—All values are presented as means ± S.E. Data were analyzed with GraphPad Prism 5.01 software using paired or unpaired Student's *t* test (for comparison of two groups) or one-way analysis of variance in combination with Bonferroni's multiple comparison post test (for comparison of three or more groups). For the statistical evaluation of distributions, the contingency test χ^2 was used. A p value ≤ 0.05 was considered statistically significant.

Results

Generation of a Gskip KO Mouse—The human GSKIP gene (also known as C14orf129 or HSPC120) encodes four alternatively spliced transcripts (National Center for Biotechnology Information (NCBI)). Splice variant 1 is the longest; the others differ only in their 5′-UTR as compared with transcript 1. Only a single transcript is expressed from the mouse *Gskip* gene (4933433P14Rik). For the generation of a conditional *Gskip* knock-out mouse, the Cre/loxP system was used (Fig. 1). Exon 2 of the *Gskip* gene contains the start codon and encodes the PKA-binding domain and 86 of the total of 139 amino acids. Exon 2 was flanked by loxP sites and thereby targeted for Cre-mediated deletion (Fig. 1*A*). Recombinant ES cells were identified via Southern blotting (Fig. 1*B*). The successful deletion of *Gskip* was confirmed at DNA (Fig. 1*C*), mRNA (Fig. 1*D*), and protein levels (Fig. 1*E*) in tissues of newborn (P0) mice.

Hemizygosity of Gskip Affects RNA but Not Protein Expression Levels—*Gskip* mRNA levels in adult *Gskip*$^{+/-}$ mice were significantly down-regulated in heart, lung, liver, brain, pancreas, kidney cortex, and spleen, with the strongest reduction appearing in the lung (Fig. 2*A*). In contrast, of all the tissues that were analyzed in *Gskip*$^{+/-}$ mice, only the renal medulla exhibited changes in GSKIP protein levels, where expression was reduced (Fig. 2*B*). Hence, hemizygosity in *Gskip*$^{+/-}$ animals does not affect GSKIP protein levels in most tissues. In line with these data, *Gskip*$^{+/-}$ mice did not exhibit any overt phenotype.

Gskip Deficiency Causes Perinatal Lethality—Timed matings between heterozygous *Gskip*$^{+/-}$ animals were set up to analyze *Gskip*$^{-/-}$ embryos at different developmental stages. The expected Mendelian ratios of wild type to heterozygous to homozygous knock-out mice of 1:2:1 were observed up to embryonic day 16.5 (E16.5; Table 1). The number of the *Gskip*$^{-/-}$ embryos decreased significantly after E16.5. Although many *Gskip*$^{-/-}$ embryos were still alive at E18.5, the embryos rapidly died within 5–30 min after Caesarean section, whereas wild type and heterozygous controls survived (Table 1). At parturition (P0), no viable GSKIP$^{-/-}$ embryos were detectable. At P0, maternal cannibalism could not be excluded and may have led to an underrepresentation of *Gskip*$^{-/-}$ embryos. Therefore, parturition appears to be the critical time point in the lethality of *Gskip*-deficient mice. The loss of GSKIP causes perinatal lethality and is not compatible with life.

Gskip$^{+/+}$ (n = 43) and *Gskip*$^{-/-}$ (n = 42) E18.5 embryos were genotyped for the presence of the Y chromosome-specific gene *Sry*. Male (*Sry*-positive) and female embryos were present in the tested groups in a similar distribution of 1:1. This indicates that the *Gskip*$^{-/-}$ phenotype in mice is sex-independent (data not shown).

Gskip-deficient Mice Do Not Initiate Breathing at Birth—The cause of the perinatal lethality seemed to be acute respiratory distress marked by cyanosis. All *Gskip*$^{-/-}$ embryos at E18.5 appeared cyanotic and pale (Fig. 3*A*, *upper*). Visual inspection of the organs of *Gskip*$^{-/-}$ mice at E18.5 did not reveal aberrations that could obviously explain the lung phenotype: *e.g.* the diaphragm appeared normal, and gross histological abnormalities did not appear in an analysis of Azan-stained E18.5 whole-body sections in different planes (Fig. 3*A*, *lower*). In addition, no significant changes in body weight were noticed between wild type, heterozygous, and *Gskip*$^{-/-}$ embryos at E18.5 or at P0 (Fig. 3*B*). E18.5 *Gskip*$^{-/-}$ mice exhibited distinct gasping movements and costal retraction, indicating a normal neuromuscular function and respiratory drive. However, a marked reduction in breathing frequency, usually in excess of 90%, was observed as compared with wild type littermates. Despite extensive efforts to breathe, all *Gskip*$^{-/-}$ mice died within 30 min of delivery.

As residual air remains in the lung even after death, it causes the tissue to float on a liquid PBS surface. This permits the amount of air in the lung to be used as an indicator of the efficiency of breathing prior to death. The lungs were dissected, weighed, and measured for their ability to float on PBS (Fig. 3, *C* and *D*). Only 4.2% out of 24 tested *Gskip*$^{-/-}$ lungs floated on a

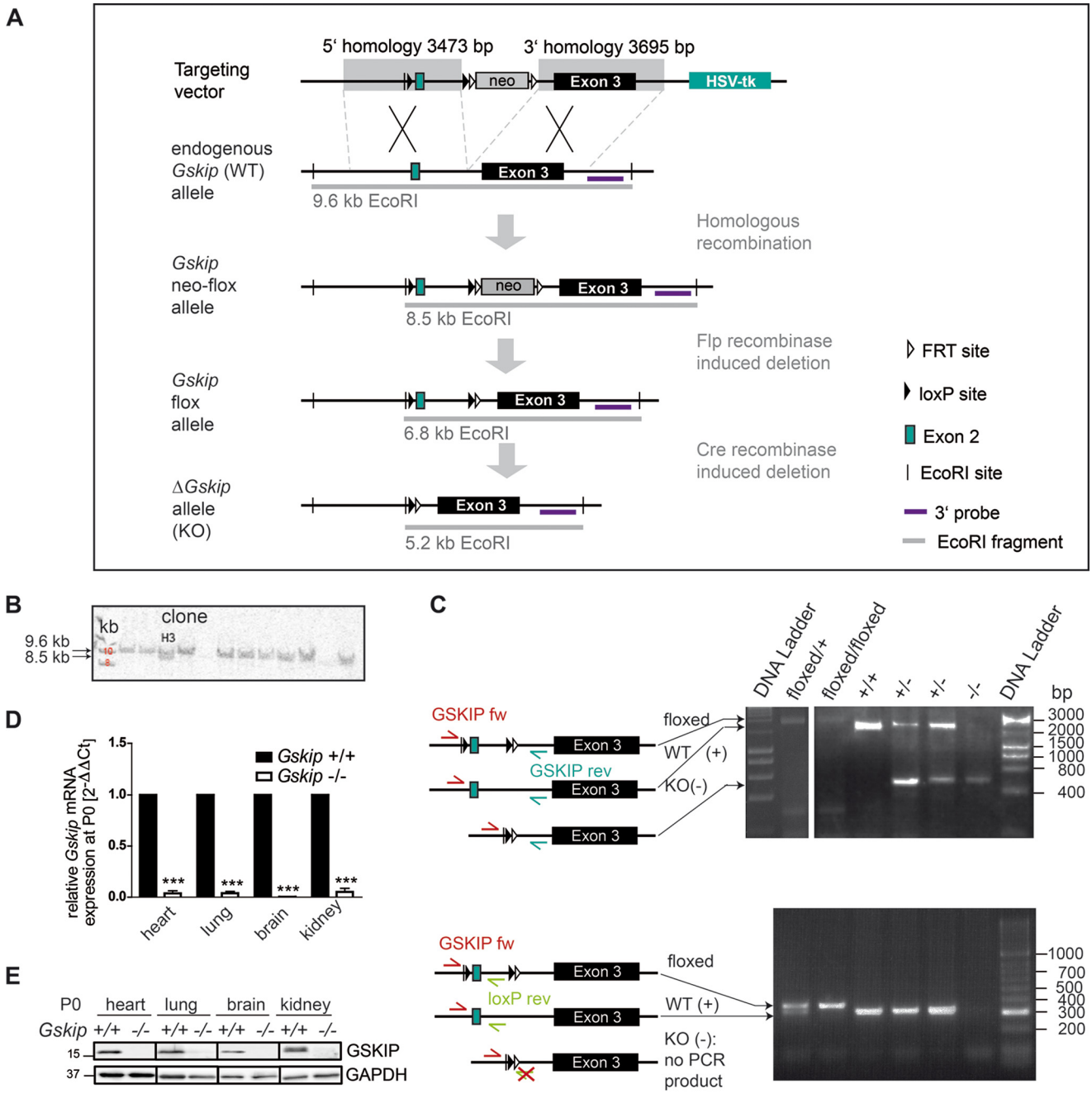

FIGURE 1. **Generation of conditional *Gskip* knock-out mice.** *A*, targeting strategy. Exon 2 of *Gskip* was targeted for loxP-mediated excision upon Cre recombination. The 3′ probe for Southern blot analysis is indicated as a *purple bar*. *B*, identification of recombinant ES cell clones. Genomic DNA from selected ES cell clones was digested with EcoRI, and fragments were analyzed by Southern blotting using a 3′ XhoI/BamHI probe. For clone H3, site-specific recombination of the target vector was detected as indicated by an 8.5-kb fragment, arising from an additional BamHI site integrated together with the targeted mutation. The 8- and 10-kb bands of the DNA marker are highlighted in *red*. *C*, PCR for the determination of genotypes. The combination of two PCRs allowed for clear genotype assignment (GSKIP-fw, *red*; GSKIP-rev, *blue*; loxP-rev, *green*). DNA fragment sizes are indicated. *D*, *Gskip* mRNA expression in P0 mouse tissue relative to *Gapdh* mRNA expression. Signals obtained by RT-PCR analyses for *Gskip*$^{-/-}$ were normalized to wild type (*Gskip*$^{+/+}$); $n \geq 5$. *E*, GSKIP protein expression in P0 *Gskip*$^{+/+}$ and *Gskip*$^{-/-}$ mice. *Upper panel*, densitometric analysis of GSKIP protein expression relative to GAPDH. Signals obtained for *Gskip*$^{-/-}$ were normalized to *Gskip*$^{+/+}$; $n \geq 11$. *Lower panel*, the indicated tissues from P0 mice were lysed, and proteins were separated by 12% SDS-PAGE. GSKIP and, as a loading control, GAPDH were detected. Representative Western blots are shown. *Error bars* indicate mean ± S.E. Data were analyzed using paired Student's *t* test. ***, $p \leq 0.001$.

PBS surface (Fig. 3*D*), pointing to lung atelectasis. These results indicate that cyanosis resulted from a failure of lung inflation in the *Gskip*$^{-/-}$ mice, and most likely a consequent reduction of oxygen diffusion into the blood. No significant alterations were noticed in postmortem lung weight to body weight ratios at E18.5, indicating that pulmonary hypo- or hyperplasia was absent in *Gskip*$^{-/-}$ mice (Fig. 3*C*).

Gskip$^{-/-}$ *Mice Display a Secondary Cleft Palate*—In addition to the lung phenotype, an anatomical abnormality of the secondary palate was consistently detected in all *Gskip*$^{-/-}$ mice. Histological examination of H&E-stained E16.5 and E18.5 mouse skull sections revealed a pronounced palatal cleft (Fig. 4*A*). In *Gskip*$^{-/-}$ mice, the secondary palatal shelf formation is disturbed in the upper jaw and the two lateral hard palatal

shelves do not fuse, resulting in no separation between the nasal and oral cavities. In wild type controls, the two lateral maxillary palatal paired shelves were fused and the midline epithelial seam disappeared at E16.5 and E18.5 (Fig. 4*A*). Palatal shelf development takes place between E12.5 and E15.5 (30); in wild type mice, the closure of the two lateral palatal bones is completed by E16.5, as confirmed by a histological analysis of wild type control mice. Our results show that GSKIP is essential for proper palatal shelf formation and suggest that the palatal cleft defect observed in *Gskip*$^{-/-}$ mice at least contributes to the defect in breathing that causes lethality.

The open connection between the nasal and the oral cavities compromises both resonant control and intraoral pressure, making it impossible for the mice to cry or suckle. This explains why newborn *Gskip*$^{-/-}$ mice did not emit sounds upon soft pressure of their tail, in contrast to the wild type. In wild type animals, an inability to suckle or vocalize ultimately leads to death by starvation, but this is not relevant in *Gskip*$^{-/-}$ mice due to their early perinatal death, which occurs before initiation of food intake.

On the molecular level, the developmental processes mediating elevation, rotation, and fusion of the palatal shelves involve Shh/Ihh, TGFβ, bone morphogenetic protein (BMP), and Wnt signaling (30, 31). Palatal clefting has been linked to disruptions of various genes that encode components of the Wnt signaling pathway (31–34). Intriguingly, the observed palatal shelf malformation in *Gskip*$^{-/-}$ mice at least partially phenocopies that observed in *Gsk3β*, *Lrp6* (15), *Gpr177* (16), *Wnt5a-* (17), and *Wnt9b-* (18) deficient mice. GSK3β is an intrinsic regulator of palatal shelf elevation (35), and the inactivation of GSK3β in the palatal epithelium of mice causes a cleft palate phenotype (36) resembling that of the *Gskip*$^{-/-}$ mice.

As increased Wnt and decreased Shh signaling inhibit GSK3β-dependent palatal bone ossification (37), we studied this feature in the *Gskip*$^{-/-}$ mice. We performed whole-mount Alizarin red/Alcian blue staining of the upper skull with an emphasis on the secondary palatal bone and cartilage structures surrounding the cleft area. The properties of the dyes account for the characteristic color pattern seen in Fig. 4*B* for *Gskip*$^{+/+}$ specimen. Calcific deposition, such as that found in bones, appears purple (stained by Alizarin red), whereas cartilage is stained in blue as a glycan-rich structure by the acidic dye Alcian blue. In *Gskip*$^{-/-}$ mice, the purple border along the bones was less pronounced, indicating a delay in ossification as compared with wild type animals (Fig. 4*B*). In addition, the skulls of *Gskip*$^{-/-}$ animals exhibited invagination-like elevated cartilage structures along the lateral hard palate fusion line in the anterior direction (*white arrows*); these were not apparent

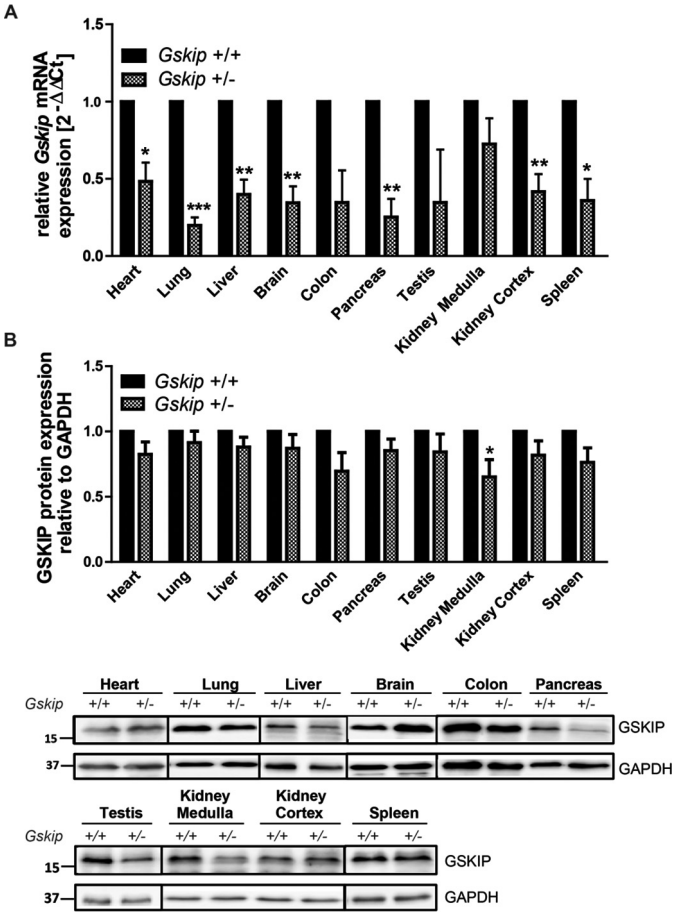

FIGURE 2. **Loss of one allele of GSKIP reduces mRNA but not protein abundance.** *A*, mRNA expression of *Gskip* relative to *Gapdh* in adult mouse tissues. Signals of mRNA from *Gskip*$^{-/-}$ mice were normalized to wild type (*Gskip*$^{+/+}$). $n \geq 4$. *B*, GSKIP protein expression in adult *Gskip*$^{+/+}$ and heterozygous *Gskip*$^{+/-}$ mice. *Upper panel*, densitometric analysis of GSKIP protein expression relative to GAPDH. *Gskip*$^{-/-}$ was normalized to *Gskip*$^{+/+}$. $n \geq 8$ ($n = 3$ for testis). *Lower panel*, representative Western blots showing the GSKIP and GAPDH expression in adult tissue lysates. Lysates were separated by 12% SDS-PAGE. GAPDH was used as a loading control. *Error bars* indicate mean ± S.E. Data were analyzed using Student's *t* test. *, $p \leq 0.05$; **, $p \leq 0.01$; ***, $p \leq 0.001$.

TABLE 1

Genotype analysis of embryos at different developmental stages

Genotype ratio distributions were calculated from offspring of *Gskip*$^{+/-}$ × *Gskip*$^{+/-}$ matings. Percentages were calculated for all three genotypes and compared with the expected Mendelian ratio. Embryos from at least 10 litters were included for each embryonic stage. χ^2 test was used for the statistical comparison of absolute numbers of the observed distributions with the expected Mendelian distribution. *, $p \leq 0.05$; ***, $p \leq 0.001$. #, died within a few min or found dead; ns: not significant.

Embryonic stage (E)	*Gskip*$^{+/+a}$	*Gskip*$^{+/-b}$	*Gskip*$^{-/-c}$	Total embryo number	χ^2 test (p)
	%	%	%		
E11.5	26	51	23	66	0.9114 ns
E12.5	32	42	26	118	0.4645 ns
E14.5	23	52	25	71	0.9170 ns
E16.5	28	45	27	73	0.8029 ns
E18.5	29	53	18#	425	0.0473*
P0	22	66	12#	99	0.0301*
P28–35	47	53	0	373	<0.0001***

[a] Mendelian ratios expected: 25 (1).
[b] Mendelian ratios expected: 50 (2).
[c] Mendelian ratios expected: 25 (1).

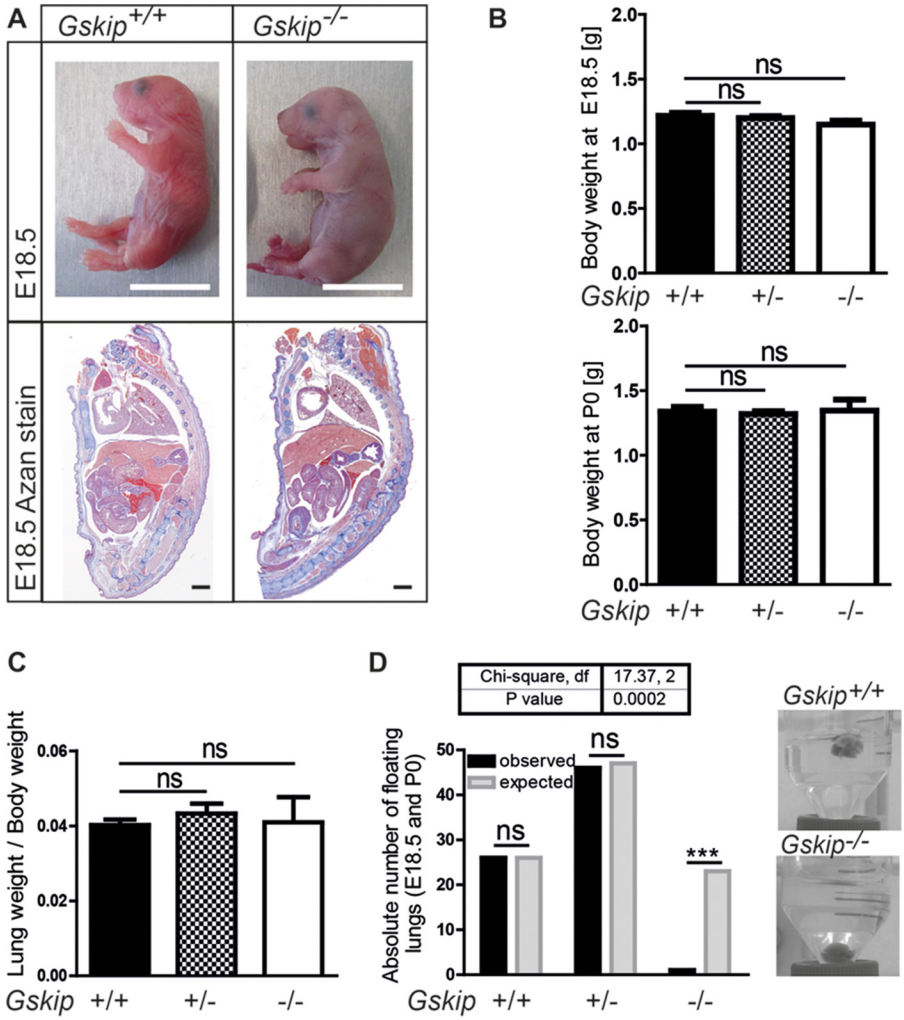

FIGURE 3. **Phenotype analysis of *Gskip*$^{-/-}$ embryos.** *A*, *upper panel*, representative images of wild type (*Gskip*$^{+/+}$) and knock-out (*Gskip*$^{-/-}$) embryos at embryonic stage E18.5. *Scale bar*, 1 cm. *Lower panel*, representative images sowing Azan-stained whole-body paraffin sections of E18.5 specimens. *Scale bar*, 1 mm. *B*, body weight comparison of *Gskip*$^{+/+}$, *Gskip*$^{+/-}$, and *Gskip*$^{-/-}$ littermates at E18.5 ($n \geq 16$ for each group; *upper panel*) and P0 ($n \geq 6$ for each group; *lower panel*). *Error bars* indicate mean ± S.E. Data were analyzed using one-way of variance. *C*, lung weight to body weight ratio. Wet lung weights and body weights were determined at E18.5 ($n \geq 6$ for each group), and ratios were calculated. *Error bars* indicate mean ± S.E. Data were analyzed using one-way of variance. *D*, the ability of E18.5 and P0 lungs to float on PBS surfaces was tested, and the number of floating lungs was compared with the expected number (100% of all tested lungs) for each genotype. $n \geq 24$ for each group. Data were analyzed using Fisher's exact test. ***, $p \leq 0.001$. *ns*, not significant. *df*, degrees of freedom.

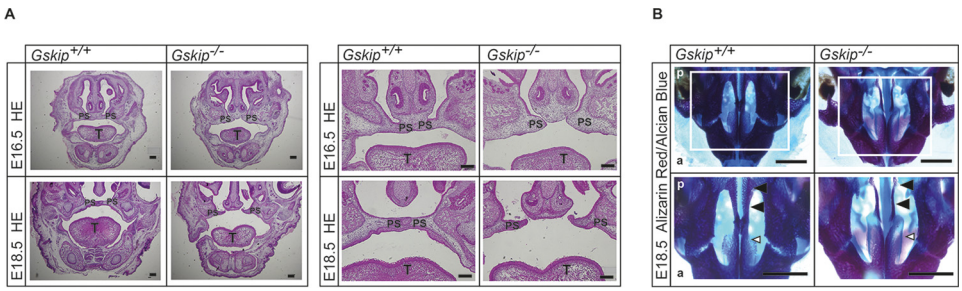

FIGURE 4. **Loss of *Gskip* causes a cleft palate and delayed ossification along the secondary palate fusion site in the mouse upper jaw.** *A*, representative H&E-stained coronal sections of paraffin-embedded E16.5 and E18.5 wild type (*Gskip*$^{+/+}$) and knock-out (*Gskip*$^{-/-}$) skulls. *Scale bar*, 200 μm. *T*, tongue; *PS*, palatal bone shelves. *B*, whole-mount Alizarin red/Alcian blue staining of dissected, eviscerated mouse skulls at E18.5 comparing *Gskip*$^{+/+}$ and *Gskip*$^{-/-}$ mice. Representative images are shown. $n = 5$. *Upper panels*, overview. *Lower panels*, magnification from region indicated by the *white boxes*. *Black arrows*, border of palatal bones. *White arrows*, anterior lateral hard palate fusion line. *p*, posterior; *a*, anterior. *Scale bar*: 1 mm.

in wild type littermates. The major difference from the wild type was the strikingly reduced amount of purple structures in *Gskip*$^{-/-}$ mice, indicative of impaired ossification within the secondary palatal shelf fusion area. Collectively, these results show that GSKIP plays a critical role in coordinating secondary palate formation and ossification.

A visible inspection of rib cage movements did not reveal differences that would point to a generalized bone defect in the

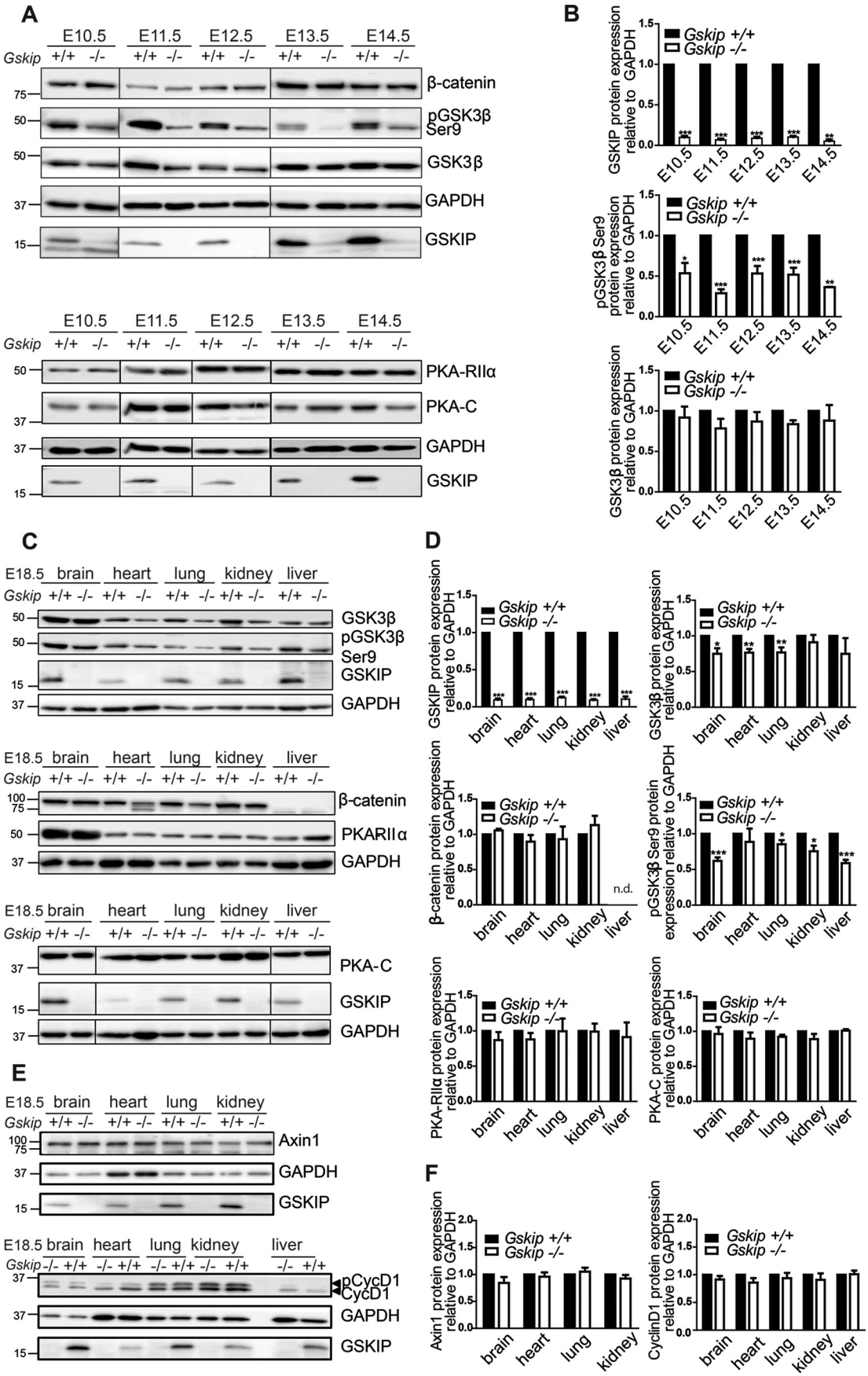
A
E10.5 E11.5 E12.5 E13.5 E14.5
Gskip +/+ -/- +/+ -/- +/+ -/- +/+ -/- +/+ -/-
β-catenin
pGSK3β Ser9
GSK3β
GAPDH
GSKIP
PKA-RIIα
PKA-C
B
GSKIP protein expression relative to GAPDH
pGSK3β Ser9 protein expression relative to GAPDH
GSK3β protein expression relative to GAPDH
Gskip +/+
Gskip -/-
C
E18.5 brain heart lung kidney liver
Axin1
pCycD1
CycD1
D
β-catenin protein expression relative to GAPDH
PKA-RIIα protein expression relative to GAPDH
PKA-C protein expression relative to GAPDH
pGSK3β Ser9 protein expression relative to GAPDH
n.d.
E
F
Axin1 protein expression relative to GAPDH
CyclinD1 protein expression relative to GAPDH

Gskip$^{-/-}$ mice. Therefore, bone mineralization and ossification are most likely not compromised outside the upper jaw. This is supported by the observation that body size and weight are not affected in *Gskip*$^{-/-}$ mice.

Loss of Gskip Causes a Reduction of the Phosphorylation of GSK3β at Ser-9—We next evaluated the molecular mechanisms that might underlie the critical functions of GSKIP during development that we had observed. We have previously shown that the overexpression of GSKIP in cultured cells facilitates the PKA phosphorylation and thus inhibition of GSK3β at Ser-9 (6), suggesting a critical role for GSKIP in GSK3β signaling. We therefore analyzed the Ser-9 phosphorylation status of GSK3β at different stages of embryonic development (E10.5, E11.5, E12.5, E13.5, E14.5) in *Gskip*$^{-/-}$ mice and controls. Remarkably, the Ser-9 phosphorylation of GSK3β was reduced by 50–70% in *Gskip*$^{-/-}$ mice as compared with wild type controls (Fig. 5, *A* and *B*), indicating an increase in GSK3β activity upon GSKIP depletion as compared with wild type controls. The ratios of phosphorylated and inactive GSK3β to total (both active and inactive) GSK3β were 0.58 ± 0.11 at E10.5, 0.37 ± 0.02 at E11.5, 0.68 ± 0.06 at E12.5, 0.38 ± 0.19 at E13.5, and 0.60 ± 0.08 at E14.5. The observations cannot be explained by the loss of PKA subunits, as the expression of the catalytic or the regulatory RIIα subunits of PKA was unaltered in the *Gskip*$^{-/-}$ mice. GSKIP only binds RII but not RI subunits of PKA (6). Ser-9 phosphorylation was also reduced at E18.5 (Fig. 5, *C* and *D*). Of note, in contrast to earlier stages of development, the E18.5 tissues displayed a reduction in the level of non-phosphorylated GSK3β protein. Hence, the ratio of inactive, Ser(P)-9 GSK3β to total (both active and inactive) GSK3β was 1.00 ± 0.06 on average in organs from E18.5, indicating that at this stage, the overall level of GSK3β activity is decreased. The expression levels of the protein components of the Wnt signaling pathway, including β-catenin, Axin1, as well as the Wnt targeting gene cyclin D1, were unaltered upon depletion of GSKIP (Fig. 5, *C–F*). In particular, the fact that β-catenin levels are unaltered is in line with the presence of GSK3β in the mostly inactive form. If active, GSK3β would phosphorylate β-catenin, which would in turn lead to its degradation.

To analyze the influence of GSKIP in a homogenous primary cell population, we turned to *Gskip*$^{-/-}$ mouse embryonic fibroblasts, generated from E12.5 embryos. The results were analogous to those obtained with mouse embryos at early stages (E10.5, E11.5, E12.5, E13.5, E14.5); although *Gskip* depletion reduced the phosphorylation of GSK3β at Ser-9 2.5-fold, it did not influence the protein expression of PKA subunits or of components of the Wnt signaling pathway (data not shown).

Collectively, our results demonstrate a critical role of GSKIP in cleft palate formation and provide strong evidence for an indispensable role of GSKIP for postnatal life. GSKIP mediates its effects at least partially through modulation of the activity of GSK3β during development.

Discussion

This work shows that the loss of the *Gskip* gene in mice causes developmental defects leading to a cleft palate and perinatal lethality caused by respiratory distress. In humans, the anatomical dysfunction caused by a secondary cleft palate is known as velopharyngeal insufficiency and involves problems with breathing, eating, hearing, and speech; treatment comprises speech therapy and surgery (38–40). Hemifacial microsomia (Goldenhar syndrome) is a human craniofacial abnormality that mainly affects the ear, mandible, muscle, and facial soft tissues and is in severe cases associated with tracheal obstruction and inadequate breathing (41). A genome-wide linkage study of affected families linked hemifacial microsomia to a region of ~10.7 centimorgans on chromosome 14q32, between microsatellite markers D14S987 (14:96128759–96129066) and D14S65 (14:97155145–97155291) (42). The GSKIP gene is located at 14:96363452–96387290 (NCBI), which places it in between these two microsatellites. These observations together with the results reported here indicate that the GSKIP gene is essential for normal craniofacial development. A dysfunction or loss of the gene may even cause hemifacial microsomia. In contrast, a duplication of the chromosomal region 14q32.13-q32.2, which encodes GSKIP and other proteins, has been associated with myeloid malignancies (7), emphasizing the important physiological function of the protein.

Prior to this study, the role of the GSKIP protein within the context of the whole organism was completely unknown. We show here that GSKIP controls GSK3β activity *in vivo*. GSK3β is constitutively active, and its activity is regulated by a combination of phosphorylation and sequestration by GSK3β-binding proteins (11). The loss of GSKIP reduces the phosphorylation of GSK3β at Ser-9 up to developmental stage E14.5. Decreased Ser-9 phosphorylation increases the activity of GSK3β (43). At the time point of death at E18.5/P0, GSK3β activity decreased again in the *Gskip*$^{-/-}$ tissues as a result of low Ser-9 phosphorylation and a decrease in the level of total GSK3β. Thus GSKIP modulates GSK3β activity and protein expression level during embryonic development.

The *Gskip*$^{-/-}$ phenotype resembles that of *Gsk3β*$^{-/-}$ mice with regard to the features of cleft palate and incomplete palatal bone ossification. The secondary palate of *Gsk3β*$^{-/-}$ mice is incompletely closed, indicating that GSK3β is essential for normal mammalian craniofacial development (36). Palatal mesenchyme-specific *Gsk3β* deficiency does not induce a palatal cleft in mice, whereas a deficiency of *Gsk3β* in the palatal epithelium causes palatal clefting due to the failure of palate elevation after

FIGURE 5. **The loss of the GSKIP protein reduces the phosphorylation of GSK3β at Ser-9 at different embryonic stages but does not affect expression levels of PKA subunits or components of the Wnt signaling pathway.** Western blot analyses of lysates from wild type (*Gskip*$^{+/+}$) and knock-out (*Gskip*$^{-/-}$) mice were performed. Proteins (15 μg) were separated by 12% SDS-PAGE. The indicated proteins were detected, and GAPDH was included as a loading control. *A*, *C*, and *E*, lysates of whole embryos (*A*) or E18.5 tissues (*C* and *E*) were assayed for β-catenin, pGSK3β Ser-9, GSK3β, regulatory RIIα, and catalytic C subunits of PKA, Axin1, cyclin D1, and GSKIP protein expression. Representative blots are shown. *B*, *D*, and *F*, densitometric analysis of protein expression relative to GAPDH. *Gskip*$^{-/-}$ was normalized to *Gskip*$^{+/+}$. $n \geq 6$ (*B* and *D*); $n \geq 3$ (*F*). *n. d.*, not detectable. *Error bars* indicate mean ± S.E.. Data were analyzed using paired Student's *t* test; *, $p \leq 0.05$; **, $p \leq 0.01$; ***, $p \leq 0.001$.

E14.5 (35). However, *Gsk3β* deletion has additional effects; it also leads to hypertrophic cardiomyopathy secondary to cardiomyoblast hyperproliferation, which is associated with the increased expression and nuclear localization of GATA4, cyclin D1, and c-Myc, three regulators of proliferation (44). *Gsk3β*$^{-/-}$ embryos display ventricular septal defects. Cardiac patterning defects (44) and severe hepatic necrosis (45) cause the conditional *Gsk3β*$^{-/-}$ mice to die at around E13.5. *Gskip*$^{-/-}$ mice die later (E18.5/P0). They do not display obvious cardiac defects. This difference from the *Gsk3β*$^{-/-}$ mice may be explained by the expression level of GSKIP in the heart, which is lower than in other tissues. *Gskip*$^{-/-}$ mice struggle from respiratory dysfunction when born and do not manage to initiate breathing *ex utero*. The expression of constitutively active GSK3β in knock-in mice expressing an enzyme that cannot be phosphorylated at Ser-9 has a different outcome than the loss of GSKIP. These knock-in mice are not impaired in their development and are viable, but exhibit hyperactive behavior (46); however, craniofacial abnormalities have not been reported. Knock-in mice with a postnatal overexpression of constitutively active GSK3β-S9A show impaired postnatal neuron maturation and differentiation, resulting in reduced brain volume due to a decrease in the size of the somatodendritic compartment (47). Conditional *Gsk3α*$^{-/-}$ mice are viable and fertile and are born at expected Mendelian ratios (44). The differences between the *Gskip*$^{-/-}$ and *Gsk3β*$^{-/-}$ phenotypes are not surprising, given that GSKIP is one scaffolding protein that influences the localization of GSK3β and some of its protein-protein interactions; GSK3β also interacts with Axin and AKAP220, and these functions might be preserved or enhanced after the loss of GSKIP.

GSKIP is also a scaffold for PKA. In its basal state, the PKA holoenzyme is composed of two regulatory (R) and two catalytic (C) subunits. The binding of cAMP to the R subunits triggers the activation of PKA and the release of its C subunits, which then phosphorylate nearby substrates (1, 3, 5, 48, 49). The loss of the catalytic Cβ subunits (*Prkacb*) or of RII subunits (*Prkar2a* and *Prkar2b*) of PKA does not affect viability and fertility, whereas the deletion of the widely expressed catalytic Cα (*Prkaca*) or regulatory RIα (*Prkar1a*) subunits is embryonically lethal. GSKIP binds PKA RIIα subunits (K_D = 5 nM) and RIIβ subunits (K_D = 43 nM) with a somewhat lower efficiency (6), so a *Gskip*$^{-/-}$ phenotype might be expected to resemble the knock-out of *Prkar2a* and *Prkar2b*. However, the loss of *Gskip* obviously has a far more pronounced effect, which results in perinatal lethality. The loss of *Gskip* most likely displaces not only RII subunits from their cognate location but also the catalytic subunits of PKA, which may then have effects as strong as the loss of the C subunits itself, *i.e.* embryonic lethality. The only AKAP that has previously been implicated in craniofacial development is AKAP95. The knock-out of the *Akap8* gene, which encodes Akap95, is not critical for palatogenesis in itself; notably, however, a double knock-out of the genes encoding AKAP95 and the ATP-dependent microtubule depolymerizing protein fidgetin induced palatal clefting in mice (50). AKAP95 is a nuclear protein, suggesting that a specific localization of PKA by an AKAP within the nucleus may not be required to coordinate proper craniofacial development. In contrast, as GSKIP is a cytosolic protein, the coordination of PKA signaling by GSKIP in the cytosol may be involved in the coordination of proper craniofacial development.

In summary, our newly developed knock-out model provides the first insights into the functions of GSKIP *in vivo*. Our results demonstrate an unexpected role of GSKIP in craniofacial development and provide strong evidence that it plays a regulatory role in controlling GSK3β activity throughout development and thereby palatal shelf fusion and ossification.

Author Contributions—V. A. D. conducted most of the experiments and wrote a large part of the paper. P. S. and K. P. K. designed and PS developed the Gskip$^{-/-}$ mouse model. C. D. conducted all experiments regarding histology. S. B. advised on immunohistochemical experiments and analyzed the results. E. K. designed the project, supported the collaboration, and wrote the manuscript with V. A. D.

Acknowledgments—We gratefully appreciate the advice of Charlotte Chaimowicz on embryo analysis and Laura Michalick for functional assessment of the lung as well as the technical assistance of Beate Eisermann and Andrea Geelhaar. We thank Russ Hodge for critically reading the manuscript.

References

1. Taylor, S. S., Ilouz, R., Zhang, P., and Kornev, A. P. (2012) Assembly of allosteric macromolecular switches: lessons from PKA. *Nat. Rev. Mol. Cell Biol.* **13,** 646–658
2. Taylor, S. S., Zhang, P., Steichen, J. M., Keshwani, M. M., and Kornev, A. P. (2013) PKA: lessons learned after twenty years. *Biochim. Biophys. Acta* **1834,** 1271–1278
3. Skroblin, P., Grossmann, S., Schäfer, G., Rosenthal, W., and Klussmann, E. (2010) Mechanisms of protein kinase A anchoring. *Int. Rev. Cell Mol. Biol.* **283,** 235–330
4. Dema, A., Perets, E., Schulz, M. S., Deák, V. A., and Klussmann, E. (2015) Pharmacological targeting of AKAP-directed compartmentalized cAMP signalling. *Cell. Signal.* **27,** 2474–2487
5. Langeberg, L. K., and Scott, J. D. (2015) Signalling scaffolds and local organization of cellular behaviour. *Nat. Rev. Mol. Cell Biol.* **16,** 232–244
6. Hundsrucker, C., Skroblin, P., Christian, F., Zenn, H. M., Popara, V., Joshi, M., Eichhorst, J., Wiesner, B., Herberg, F. W., Reif, B., Rosenthal, W., and Klussmann, E. (2010) Glycogen synthase kinase 3β interaction protein functions as an A-kinase anchoring protein. *J. Biol. Chem.* **285,** 5507–5521
7. Saliba, J., Saint-Martin, C., Di Stefano, A., Lenglet, G., Marty, C., Keren, B., Pasquier, F., Valle, V. D., Secardin, L., Leroy, G., Mahfoudhi, E., Grosjean, S., Droin, N., Diop, M., Dessen, P., Charrier, S., Palazzo, A., Merlevede, J., Meniane, J. C., Delaunay-Darivon, C., Fuseau, P., Isnard, F., Casadevall, N., Solary, E., Debili, N., Bernard, O. A., Raslova, H., Najman, A., Vainchenker, W., Bellanné-Chantelot, C., and Plo, I. (2015) Germline duplication of *ATG2B* and *GSKIP* predisposes to familial myeloid malignancies. *Nat. Genet.* **47,** 1131–1140
8. Chou, H. Y., Howng, S. L., Cheng, T. S., Hsiao, Y. L., Lieu, A. S., Loh, J. K., Hwang, S. L., Lin, C. C., Hsu, C. M., Wang, C., Lee, C. I., Lu, P. J., Chou, C. K., Huang, C. Y., and Hong, Y. R. (2006) GSKIP is homologous to the Axin GSK3β interaction domain and functions as a negative regulator of GSK3β. *Biochemistry* **45,** 11379–11389
9. Bijur, G. N., and Jope, R. S. (2003) Glycogen synthase kinase-3β is highly activated in nuclei and mitochondria. *Neuroreport* **14,** 2415–2419
10. Beurel, E., Grieco, S. F., and Jope, R. S. (2015) Glycogen synthase kinase-3 (GSK3): regulation, actions, and diseases. *Pharmacol. Ther.* **148,** 114–131
11. Kaidanovich-Beilin, O., and Woodgett, J. R. (2011) GSK-3: functional insights from cell biology and animal models. *Front. Mol. Neurosci.* **4,** 40
12. Dajani, R., Fraser, E., Roe, S. M., Young, N., Good, V., Dale, T. C., and Pearl, L. H. (2001) Crystal structure of glycogen synthase kinase 3β: structural basis for phosphate-primed substrate specificity and autoinhibition. *Cell* **105,** 721–732

13. Logan, C. Y., and Nusse, R. (2004) The Wnt signaling pathway in development and disease. *Annu. Rev. Cell Dev. Biol.* **20,** 781–810
14. Clevers, H. (2006) Wnt/β-catenin signaling in development and disease. *Cell* **127,** 469–480
15. Song, L., Li, Y., Wang, K., Wang, Y. Z., Molotkov, A., Gao, L., Zhao, T., Yamagami, T., Wang, Y., Gan, Q., Pleasure, D. E., and Zhou, C. J. (2009) Lrp6-mediated canonical Wnt signaling is required for lip formation and fusion. *Development* **136,** 3161–3171
16. Liu, Y., Wang, M., Zhao, W., Yuan, X., Yang, X., Li, Y., Qiu, M., Zhu, X. J., and Zhang, Z. (2015) Gpr177-mediated Wnt signaling is required for secondary palate development. *J. Dent. Res.* **94,** 961–967
17. He, F., Xiong, W., Yu, X., Espinoza-Lewis, R., Liu, C., Gu, S., Nishita, M., Suzuki, K., Yamada, G., Minami, Y., and Chen, Y. (2008) Wnt5a regulates directional cell migration and cell proliferation via Ror2-mediated noncanonical pathway in mammalian palate development. *Development* **135,** 3871–3879
18. Juriloff, D. M., Harris, M. J., McMahon, A. P., Carroll, T. J., and Lidral, A. C. (2006) *Wnt9b* is the mutated gene involved in multifactorial nonsyndromic cleft lip with or without cleft palate in A/WySn mice, as confirmed by a genetic complementation test. *Birth Defects Res. A Clin. Mol. Teratol.* **76,** 574–579
19. Kohli, S. S., and Kohli, V. S. (2012) A comprehensive review of the genetic basis of cleft lip and palate. *J. Oral Maxillofac. Pathol.* **16,** 64–72
20. Juriloff, D. M., and Harris, M. J. (2008) Mouse genetic models of cleft lip with or without cleft palate. *Birth Defects Res. A Clin. Mol. Teratol.* **82,** 63–77
21. Carroll, T. J., Park, J. S., Hayashi, S., Majumdar, A., and McMahon, A. P. (2005) Wnt9b plays a central role in the regulation of mesenchymal to epithelial transitions underlying organogenesis of the mammalian urogenital system. *Dev. Cell* **9,** 283–292
22. Sadot, E., Conacci-Sorrell, M., Zhurinsky, J., Shnizer, D., Lando, Z., Zharhary, D., Kam, Z., Ben-Ze'ev, A., and Geiger, B. (2002) Regulation of S33/S37 phosphorylated β-catenin in normal and transformed cells. *J. Cell Sci.* **115,** 2771–2780
23. MacDonald, B. T., Tamai, K., and He, X. (2009) Wnt/β-catenin signaling: components, mechanisms, and diseases. *Dev. Cell* **17,** 9–26
24. Amit, S., Hatzubai, A., Birman, Y., Andersen, J. S., Ben-Shushan, E., Mann, M., Ben-Neriah, Y., and Alkalay, I. (2002) Axin-mediated CKI phosphorylation of β-catenin at Ser 45: a molecular switch for the Wnt pathway. *Genes Dev.* **16,** 1066–1076
25. Schwarz-Romond, T., Asbrand, C., Bakkers, J., Kühl, M., Schaeffer, H. J., Huelsken, J., Behrens, J., Hammerschmidt, M., and Birchmeier, W. (2002) The ankyrin repeat protein Diversin recruits Casein kinase Iε to the β-catenin degradation complex and acts in both canonical Wnt and Wnt/JNK signaling. *Genes Dev.* **16,** 2073–2084
26. Davidson, G., Wu, W., Shen, J., Bilic, J., Fenger, U., Stannek, P., Glinka, A., and Niehrs, C. (2005) Casein kinase 1γ couples Wnt receptor activation to cytoplasmic signal transduction. *Nature* **438,** 867–872
27. Lin, C. C., Chou, C. H., Howng, S. L., Hsu, C. Y., Hwang, C. C., Wang, C., Hsu, C. M., and Hong, Y. R. (2009) GSKIP, an inhibitor of GSK3β, mediates the N-cadherin/β-catenin pool in the differentiation of SH-SY5Y cells. *J. Cell. Biochem.* **108,** 1325–1336
28. Schwenk, F., Baron, U., and Rajewsky, K. (1995) A *cre*-transgenic mouse strain for the ubiquitous deletion of *loxP*-flanked gene segments including deletion in germ cells. *Nucleic Acids Res.* **23,** 5080–5081
29. Erdoğan, D. K., Kadioğlu, D., and Peker, T. (1995) Visualisation of fetal skeletal system by double staining with Alizarin red and Alcian blue. *Gazi Med. J.* 55–58
30. Funato, N., Nakamura, M., and Yanagisawa, H. (2015) Molecular basis of cleft palates in mice. *World J. Biol. Chem.* **6,** 121–138
31. Levi, B., Brugman, S., Wong, V. W., Grova, M., Longaker, M. T., and Wan, D. C. (2011) Palatogenesis: engineering, pathways and pathologies. *Organogenesis* **7,** 242–254
32. Juriloff, D. M., Harris, M. J., and Mah, D. G. (1996) The *clf1* gene maps to a 2- to 3-cM region of distal mouse chromosome 11. *Mamm. Genome* **7,** 789
33. Juriloff, D. M., Harris, M. J., and Brown, C. J. (2001) Unravelling the complex genetics of cleft lip in the mouse model. *Mamm. Genome* **12,** 426–435
34. Juriloff, D. M., Harris, M. J., Dewell, S. L., Brown, C. J., Mager, D. L., Gagnier, L., and Mah, D. G. (2005) Investigations of the genomic region that contains the *clf1* mutation, a causal gene in multifactorial cleft lip and palate in mice. *Birth Defects Res. A Clin. Mol. Teratol.* **73,** 103–113
35. He, F., Popkie, A. P., Xiong, W., Li, L., Wang, Y., Phiel, C. J., and Chen, Y. (2010) Gsk3β is required in the epithelium for palatal elevation in mice. *Dev. Dyn.* **239,** 3235–3246
36. Liu, K. J., Arron, J. R., Stankunas, K., Crabtree, G. R., and Longaker, M. T. (2007) Chemical rescue of cleft palate and midline defects in conditional GSK-3β mice. *Nature* **446,** 79–82
37. Nelson, E. R., Levi, B., Sorkin, M., James, A. W., Liu, K. J., Quarto, N., and Longaker, M. T. (2011) Role of GSK-3β in the osteogenic differentiation of palatal mesenchyme. *PLoS One* **6,** e25847
38. Shetty, N. B., Shetty, S., E, N., D'Souza, R., and Shetty, O. (2014) Management of velopharyngeal defects: a review. *J. Clin. Diagn. Res.* **8,** 283–287
39. Steinberg, B., Caccamese, J., Jr., and Padwa, B. L. (2012) Cleft and craniofacial surgery. *J. Oral Maxillofac. Surg.* **70,** e137–161
40. Capra, G., and Brigger, M. T. (2012) Surgery for velopharyngeal insufficiency. *Adv. Otorhinolaryngol.* **73,** 137–144
41. Poole, M. D. (1989) Hemifacial microsomia. *World J. Surg.* **13,** 396–400
42. Kelberman, D., Tyson, J., Chandler, D. C., McInerney, A. M., Slee, J., Albert, D., Aymat, A., Botma, M., Calvert, M., Goldblatt, J., Haan, E. A., Laing, N. G., Lim, J., Malcolm, S., Singer, S. L., Winter, R. M., and Bitner-Glindzicz, M. (2001) Hemifacial microsomia: progress in understanding the genetic basis of a complex malformation syndrome. *Hum. Genet.* **109,** 638–645
43. Frame, S., Cohen, P., and Biondi, R. M. (2001) A common phosphate binding site explains the unique substrate specificity of GSK3 and its inactivation by phosphorylation. *Mol. Cell* **7,** 1321–1327
44. Kerkela, R., Kockeritz, L., Macaulay, K., Zhou, J., Doble, B. W., Beahm, C., Greytak, S., Woulfe, K., Trivedi, C. M., Woodgett, J. R., Epstein, J. A., Force, T., and Huggins, G. S. (2008) Deletion of GSK-3β in mice leads to hypertrophic cardiomyopathy secondary to cardiomyoblast hyperproliferation. *J. Clin. Invest.* **118,** 3609–3618
45. Hoeflich, K. P., Luo, J., Rubie, E. A., Tsao, M. S., Jin, O., and Woodgett, J. R. (2000) Requirement for glycogen synthase kinase-3β in cell survival and NF-κB activation. *Nature* **406,** 86–90
46. McManus, E. J., Sakamoto, K., Armit, L. J., Ronaldson, L., Shpiro, N., Marquez, R., and Alessi, D. R. (2005) Role that phosphorylation of GSK3 plays in insulin and Wnt signalling defined by knockin analysis. *EMBO J.* **24,** 1571–1583
47. Spittaels, K., Van den Haute, C., Van Dorpe, J., Terwel, D., Vandezande, K., Lasrado, R., Bruynseels, K., Irizarry, M., Verhoye, M., Van Lint, J., Vandenheede, J. R., Ashton, D., Mercken, M., Loos, R., Hyman, B., Van der Linden, A., Geerts, H., and Van Leuven, F. (2002) Neonatal neuronal overexpression of glycogen synthase kinase-3 β reduces brain size in transgenic mice. *Neuroscience* **113,** 797–808
48. McCormick, K., and Baillie, G. S. (2014) Compartmentalisation of second messenger signalling pathways. *Curr. Opin. Genet. Dev.* **27,** 20–25
49. Walsh, D. A., Perkins, J. P., and Krebs, E. G. (1968) An adenosine 3′,5′-monophosphate-dependant protein kinase from rabbit skeletal muscle. *J. Biol. Chem.* **243,** 3763–3765
50. Yang, Y., Mahaffey, C. L., Bérubé, N., and Frankel, W. N. (2006) Interaction between fidgetin and protein kinase A-anchoring protein AKAP95 is critical for palatogenesis in the mouse. *J. Biol. Chem.* **281,** 22352–22359